IEEE Photonics Journal
An IEEE Photonics Society Publication

Open Access

III-Nitride Deep UV LED Without Electron Blocking Layer

Volume 11, Number 2, April 2019

Zhongjie Ren
Yi Lu
Hsin-Hung Yao
Haiding Sun
Che-Hao Liao
Jiangnan Dai
Changqing Chen
Jae-Hyun Ryou
Jianchang Yan
Junxi Wang
Jinmin Li
Xiaohang Li

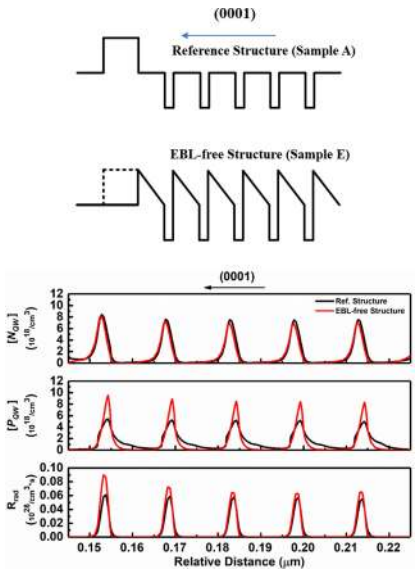

DOI: 10.1109/JPHOT.2019.2902125
1943-0655 © 2019 IEEE

III-Nitride Deep UV LED Without Electron Blocking Layer

Zhongjie Ren, Yi Lu, Hsin-Hung Yao, Haiding Sun, Che-Hao Liao, Jiangnan Dai, Changqing Chen, Jae-Hyun Ryou, Jianchang Yan, Junxi Wang, Jinmin Li, and Xiaohang Li

Advanced Semiconductor Laboratory, King Abdullah University of Science and Technology, Thuwal 23955-6900, Saudi Arabia
Research and Development Center for Solid State Lighting, Institute of Semiconductors, Chinese Academy of Sciences, Beijing 100083, China
Wuhan National Laboratory for Optoelectronics, Huazhong University of Science and Technology, Wuhan 430074, China
Department of Mechanical Engineering, Material Science and Engineering Program, Texas Center for Superconductivity at UH, and Advanced Manufacturing Institute, University of Houston, Houston, TX 77204-4006 USA

DOI:10.1109/JPHOT.2019.2902125

Manuscript received January 5, 2019; revised February 20, 2019; accepted February 24, 2019. Date of publication March 1, 2019; date of current version March 14, 2019. The work of Z. Ren, Y. Lu, H.-H. Yao, H. Sun, C.-H. Liao, and X. Li was supported in part by King Abdullah University of Science and Technology (KAUST) Baseline BAS/1/1664-01-01, KAUST CRG URF/1/3437-01-01, GCC REP/1/3189-01-01; and in part by the National Natural Science Foundation of China under Grant 61774065. The work of Y. Lu, J. Yan, J. Wang, and J. Li was supported by the National Key R&D Program of China under Grants 2016YFB0400803 and 2016YFB0400802. The work of J. Dai and C. Chen was supported in part by the Key Project of Chinese National Development Programs under Grant 2018YFB0406602 and in part by the National Natural Science Foundation of China under Grant 61774065. The work of J.-H. Ryou was supported in part by KAUST under Contract OSR-2017-CRG6-3437.02 and in part by the Texas Center for Superconductivity at the University of Houston. *(Zhongjie Ren and Yi Lu contributed equally to this work.)* Corresponding author: Xiaohang Li (e-mail: xiaohang.li@kaust.edu.sa).

Abstract: AlGaN-based deep UV (DUV) LEDs generally employ a p-type electron blocking layer (EBL) to suppress electron overflow. However, Al-rich III-nitride EBL can result in challenging p-doping and large valence band barrier for hole injection as well as epitaxial complexity. As a result, wall plug efficiency (WPE) can be compromised. Our systematic studies of band diagram and carrier concentration reveal that carrier concentrations in the quantum well and electron overflow can be significantly impacted because of the slope variation of the quantum barrier (QB) conduction and valence bands, which in turn influence radiative recombination and optical output power. Remarkably, grading the Al composition from 0.60 to 0.70 for the 12-nm-thick AlGaN QB of the DUV LED without the EBL can lead to 13.5% higher output power and similar level of overflown electron concentration ($\sim 1 \times 10^{15}/cm^3$) as opposed to the conventional DUV LED with the p-type EBL. This paradigm is significant for the pursuit of higher WPE or shorter emission wavelength for DUV LEDs and lasers, as it provides a new direction for addressing electron overflow and hole injection issues.

Index Terms: Aluminum gallium nitride, deep UV LED, electron blocking, electron containing, electron overflow.

1. Introduction

DEEP UV (DUV) sources can be utilized in numerous important applications including water and air purification, biological analysis, medical sensor, and curing. Compared to the most widely used mercury-based DUV sources, AlGaN-based semiconductor DUV light emitting diodes (LEDs) are environment-friendly, compact, and long-lasting. However, unlike the highly efficient blue LEDs, DUV LEDs still suffer from single-digit wall plug efficiency (WPE) even though the highest external quantum efficiency (EQE) is over 20% [1], [2]. Amid major WPE constraints, one is the very existence of the ubiquitous electron blocking layer (EBL). For III-nitride LEDs, electrons have much higher mobility than holes, thereby prone to flowing over the active region typically comprising multiple quantum wells (MQWs) into the p-type region [3]. The overflown electrons do not participate in radiative recombination in the active region and become wasted. Moreover, they can recombine with holes in the p-type region to reduce hole injection efficiency. Thus the electron overflow is one major contributing factors to lower WPE [4], [5]. To address the electron overflow, the EBL, commonly a wider-bandgap and higher-Al-composition layer or structure, has been employed between the p-type region and the active region [6], [7].

However, the EBL can hinder hole injection and increase serial resistance constraining the WPE due to two intrinsic material properties. First, the band alignment determines that the heterojunctions formed by InAlGaN alloys are type-I (straddling gap) [8]. This indicates that the desirable conduction band barrier of the EBL blocking electrons on the active region side also leads to simultaneous formation of a valence band barrier blocking holes on the p-type region side, thereby impeding hole injection [9], [10]. Second, excellent p-type doping is necessary for the EBL to achieve low layer resistance. However, the activation energy of the Mg acceptor in III-nitride layers increases rapidly with the Al composition, which makes the p-doping challenging for Al-rich III-nitride layers such as AlGaN [11]. For state-of-the-art DUV LEDs emitting at technically-important wavelength range of 225-280 nm, the Al compositions of the p-type AlGaN EBLs can be up to 95%, posing major challenges for the p-doping [2], [12], [13]. In short, the higher Al compositions can lead to lower hole injection efficiency in the active region and more challenging Mg activation in the EBL, which are both negative for WPE improvement. Because of the technical importance of the DUV LED, both issues of the EBL have attracted enormous interest and attention.

To address the valence band barrier issue, some researchers have employed the AlGaN/AlGaN superlattice EBL to modify the energy band to facilitate hole injection to the active region [14]. The grading EBL [15] and inverted-V-shaped graded Al-composition EBL [16] have also been put forward for their advantages on the reduction of valence band barrier. In addition, the EBL with a thin AlGaN insertion layer with a smaller energy bandgap has been utilized to acquire the intraband-tunneling-assisted hole injection, which can bring down the valence band barrier height of EBL as well as enhance the hole tunneling effect [17]. To improve the p-doping in the AlGaN EBL with higher Al compositions, researchers have proposed polarization doping to induce three-dimensional hole gas by grading the Al composition in AlGaN layer [18], [19]. Moreover, p-AlGaN/AlGaN superlattice with the average composition of 60% has been demonstrated where activation energy for Mg dopants is reduced to 17 meV [20]. Besides, Mg-delta doping [21] and Mg-Si co-doping [22], [23] have been investigated. However, those approaches could possess the optical absorption problem, suffer complex epitaxial condition, or fail to decrease the valence band barrier in the EBL. Accordingly, while the previous works on improving the EBL are meaningful and encouraging, further investigations are still required to find an effective and straightforward solution to suppress electron overflow and enhance hole injection simultaneously.

At the onset of this study, we propose that apart from continuing to optimize the *electron blocking* layer, ones could shift the research paradigm to *electron containing*: with deliberate electrostatic potential engineering, the active region shall also become the *electron containing* region to suppress electron overflow as well as simultaneously enhance hole injection. Hence, the DUV LED would have the option of relinquishing the EBL and thereby avoid the associated issues. Previously, majority of the electrostatic potential studies of the active region focused on the quantum well (QW) such as the use of step-like potentials with the goal of enhancing the electron-hole wavefunction

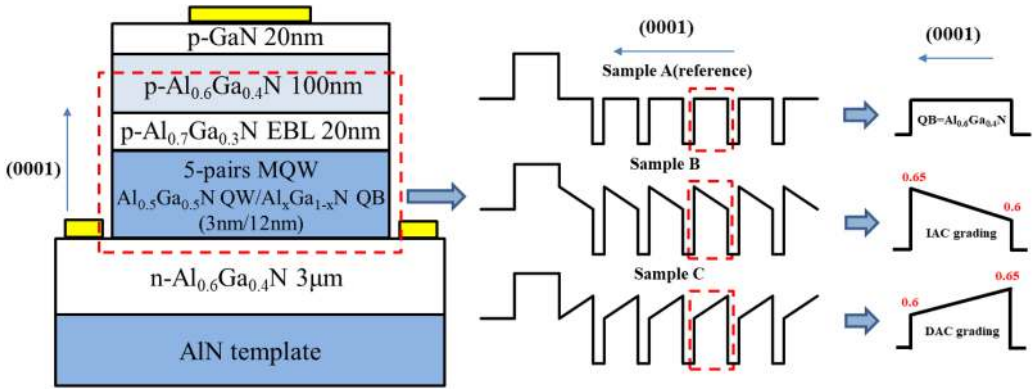

Fig. 1. The cross-sectional schematics and Al composition profiles of Samples A, B, and C with different Al-composition QB grading schemes based on the conventional DUV LED emitting at ~270 nm. Sample A is the reference without grading.

overlap for higher radiative recombination rates [24]–[26]. Besides the QWs, some studies investigated doping and changing electrostatic potentials of the quantum barrier (QB) for the controls of electron and hole quantum confinement or injection in the active region [27]–[30]. Despite these meaningful progresses, the reported devices still require the p-type AlGaN EBL.

For visible InGaN LEDs, a plurality of reports on composition grading QBs show promising outcomes such as enhanced hole injection and more uniform carrier distribution in QWs together with grading of the EBL [31], enhanced hole injection without the EBL [32], enhanced hole injection and reduced droop [33]. It is important to note that those studies mainly aim to improve hole injection instead of electron blocking. For the DUV LED, however, hole mobility is typically low single digit $cm^2/(V{\cdot}s)$ which is much smaller than that of electrons [34]–[37]. Thus, the low hole mobility and the imbalance between electron and hole mobility indicates that the electron containing/blocking must be taken into account together with hole injection for high performance devices, which would be discussed in this study.

To design the EBL-free DUV LED with similar performance to the DUV LED with the EBL, we begin with investigation of the electron containing capability amid different QB grading and their impacts on the hole injection and radiative recombination rate. With the linearly-increased Al-composition grading showing promise, we then shift the focus to conduct detailed studies of various compositional ranges to identity changing trends of the carrier concentrations and the electron containing capability. Eventually, we propose the EBL-free DUV LED structure that manifests the ability of effective suppressing electron overflow and exhibits similar or better output power. We also discuss the feasibility of the proposed method, suggesting that it is straightforward to be implemented to replace or enhance the EBL.

2. Impacts of Quantum Barrier Grading

To fundamentally investigate the electron containing capability of the QB with linearly-graded composition, we first construct three metal-polar device structures with three QB grading schemes based on the conventional DUV LED with an EBL as shown in Figure 1. Their structures are the same except the QB. The diode structure on an AlN template begins with a 3-μm-thick n-type $Al_{0.6}Ga_{0.4}N$ layer with Si doping concentration of 5×10^{18} cm^{-3}. The p-type region consists of a 20-nm-thick p-$Al_{0.7}Ga_{0.3}N$ EBL layer with Mg doping concentration of 3×10^{19} cm^{-3}, a 100-nm-thick p-$Al_{0.6}Ga_{0.4}N$ hole-injection layer with Mg doping concentration of 2×10^{19} cm^{-3}, and finally a 50-nm p-GaN contact layer with Mg doping concentration of 1×10^{20} cm^{-3}. For the device simulation, the Advanced Physical Models of Semiconductor Devices (APSYS) program is employed [38]. The 6×6 k·p model developed by Chuang [39] and Chang [40] is employed to calculate the band structures. Due to the poor hole mobility of Al-rich materials, a three-column LED structure model,

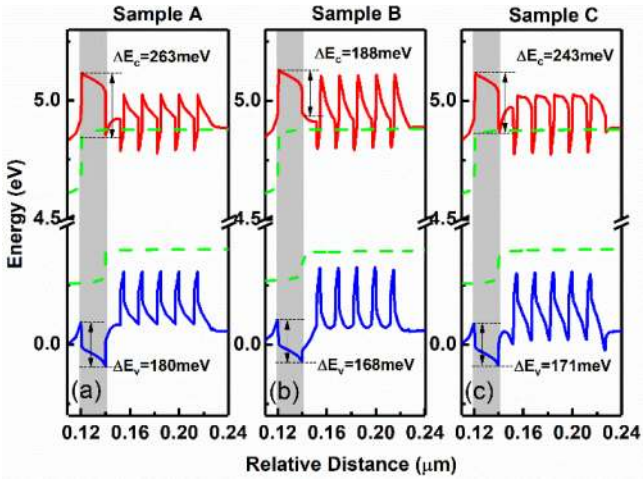

Fig. 2. Band diagrams of the active regions and the EBLs of (a) Sample A, (b) Sample B, and (c) Sample C at 90 mA. The gray area locates the EBLs with conduction and valence band offsets ΔE_c and ΔE_v.

with two n-type and one p-type contact electrodes, is used to improve lateral current spreading [41]. The LED chip size is kept at 300 $\times$ 300 μm^2 and the emission wavelength is designed to be 270 nm, a technically-important wavelength range for sterilization, sensing, and other applications. The activation energy of n-type $Al_{0.6}Ga_{0.4}N$ is set to 15 meV according to experimental data [42]. Meanwhile, the Mg activation energy of p-type $Al_{0.7}Ga_{0.3}N$ and p-type $Al_{0.6}Ga_{0.4}N$ is set to 71 [34] and 60 meV [43], respectively. The Mg activation energy of p-type GaN is set to 118 meV from a less up-to-date experimental report [44]. However, it is noted that the Mg activation energy of p-type GaN does not affect the trends or conclusions of this study. The hole and electron mobility of AlGaN is based on previous reports and the alloy mobility model inside APSYS [35]–[37].

For the active region, Samples A, B, and C all comprise five 3-nm-thick $Al_{0.5}Ga_{0.5}N$ QWs sandwiched by six 12-nm thick AlGaN QBs. The QBs have different composition grading schemes. The QBs of Sample A (reference) comprise fixed-composition $Al_{0.6}Ga_{0.4}N$. The QBs of Sample B have increased-Al-composition (IAC) linear-grading profile from 0.6 to 0.65 along the c-axis. Oppositively, the QBs of Sample C have decreased-Al-composition (DAC) linear-grading profile from 0.65 to 0.6. The Shockley-Read-Hall (SRH) recombination lifetime, the Auger recombination coefficient, the radiative recombination coefficient, and the light extraction efficiency are set to be 15 ns, 2.88 $\times$ 10^{-30} cm^6/s, 2.13 $\times$ 10^{-11} cm^3/s, and 10%, respectively [45]. The bowing factor of the bandgap and the band offset ratio of AlGaN materials are set to be 0.94 and 0.67/0.33, respectively [46]. Effective mass parameters are determined according to Punya *et al.* [47]. The interface charge densities are assumed to be 50% of total charges considering the screening effect of defects. The charge densities screened by injected carriers under forward bias are taken into account self-consistently.

Figure 2(a)–(c) show the band diagrams of Samples A, B, and C at 90 mA. The grading impacts the slope of the QB conduction and valence bands considerably. For the QB conduction band, Sample B shows steeper potential barrier due to the IAC grading as compared to Sample A, while Sample C exhibits flatter barrier due to compensation of existing interface charge by the DAC grading. For the QB valence band, however, Sample B and Sample C manifest flatter and steeper QB valence bands, respectively, which is the opposite behavior to the QB conduction bands. In addition, the QB grading can cause considerable changes to the EBL conduction and valence band offsets ΔE_c and ΔE_v since the last QB is adjacent to the EBL. ΔE_c for electron blocking in Samples A, B, and C are 263, 188, and 243 meV, respectively. Notably, Sample B possesses the smallest ΔE_c while those of Samples A and C are similar. ΔE_v related to hole injection in Sample A, B, and C are 180, 168, 171 meV, respectively. The hole barriers of Sample B and C are slightly lower than that of Sample A. If the active regions of Samples A, B, and C were the same, it would be straightforward to predict that Sample B would have the largest electron overflow and Sample C would have larger

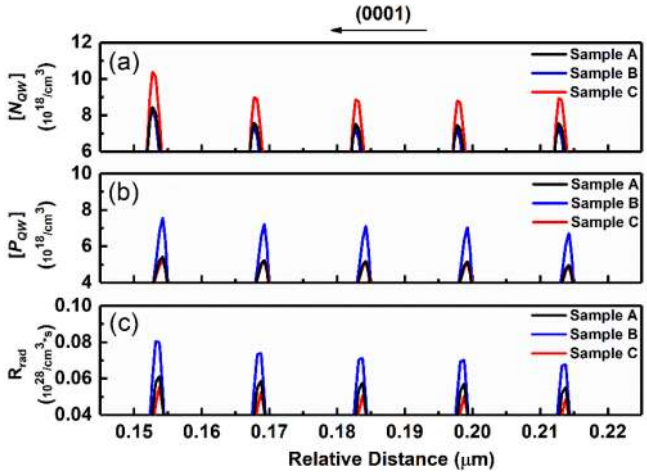

Fig. 3. (a) Electron concentration $[N_{QW}]$, (b) hole concentration $[P_{QW}]$, and (c) radiative recombination rate R_{rad} in the QWs of Samples A, B, and C at 90 mA.

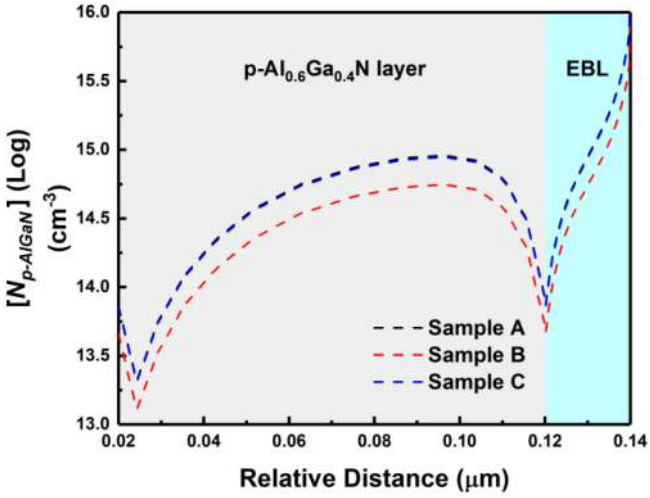

Fig. 4. Electron concentration $[N_{p-AlGaN}]$ in the p-$Al_{0.6}Ga_{0.4}N$ layer of Samples A, B, and C. The EBL is included as a position indicator.

hole concentration than Sample A in the QWs. However, they are not necessarily the case, because the slopes of the QB conduction and valence bands can strongly influence the carrier transport that is the key to the electron containing capability. The change of the QB band slope versus the end composition of the IAC grading can be quantified as shown in the Supplementary Material.

Figure 3(a)–(b) show electron concentration $[N_{QW}]$ and hole concentration $[P_{QW}]$ in the QWs from the band diagram of Figure 2. Overall, $[N_{QW}]$ is larger than $[P_{QW}]$ mainly due to the lower activation energy of electrons than holes. Specifically, Sample C has the highest average $[N_{QW}]$, Sample B has the highest average $[P_{QW}]$, and Sample A shows intermediate behavior. For electrons, the higher $[N_{QW}]$ in Sample C is attributed to the flatter QB conduction band, which is in favor of the electron injection in QWs. For Samples A and B, although Sample B has steeper QB conduction band, electrons can still overcome it due to large mobility, eventually causing $[N_{QW}]$ of Sample B to be just slightly reduced from that of Sample A. More discussion concerning the relationship between the steeper QB conduction band and $[N_{QW}]$ is below related to Figure 5(a). For holes, on the other hand, the highest $[P_{QW}]$ of Sample B is due to flatter QBs and thus lower effective transport barrier. At the same time, the slightly lower $[P_{QW}]$ in Sample C than that of Sample A can

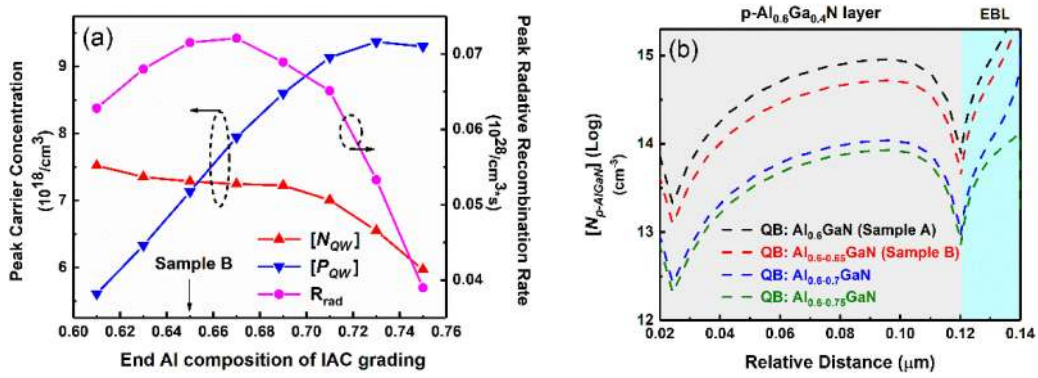

Fig. 5. (a) Peak carrier concentration and peak radiative recombination rate R_{rad} in the middle QW of the active region versus the end Al composition of the IAC grading. (b) Electron concentration $[N_{p-AlGaN}]$ in the p-$Al_{0.6}Ga_{0.4}N$ layer with different IAC grading ranges, indicating degree of electron overflow.

be explained by that the lower EBL barrier of Sample C is compensated by the steeper QB and thus higher transport barrier.

The comparisons of $[N_{QW}]$ and $[P_{QW}]$ between Samples A, B and C indicate that the slope of the QB can play a profound role in the carrier concentration in the active region [Figure 3(a) and (b)]. Moreover, it is essential to understand the electron containing capability of the active regions with different QB grading schemes. Figure 4 shows the electron concentration in the p-$Al_{0.6}Ga_{0.4}N$ layer $[N_{p-AlGaN}]$ of Samples A, B, and C as the indicator of the electron overflow. Interestingly, Sample B shows lower $[N_{p-AlGaN}]$ compared to Samples A and C despite that ΔE_c at its EBL (188 meV) is much lower than those of Samples A and C. The lower $[N_{p-AlGaN}]$ unambiguously demonstrates the electron containing ability of the active region of Sample B due to the QB IAC grading and the resulting higher QB conduction slope which makes it more difficult for electrons to transport to the p-type region.

Figure 3(c) exhibits the radiative recombination rate R_{rad} in the QWs of Samples A, B, and C. For Samples A, $[P_{QW}]$ is significantly lower than $[N_{QW}]$, but Sample C exhibits the largest imbalance. As a pair of electron and hole is required for radiative recombination, the lower $[P_{QW}]$ indicates that $[P_{QW}]$ dominates the radiative recombination, leading to lower R_{rad} for Sample A compared with Sample B. For Sample C, $[P_{QW}]$ is the lowest, leading to the lowest R_{rad}. For Sample B, $[P_{QW}]$ still dominates the radiative recombination but it is much higher and closer to $[N_{QW}]$. Thereby Sample B exhibits the highest R_{rad}, as shown in Figure 3(c).

As the QB IAC grading can lead to the electron-containing capability and the higher R_{rad} as shown by Sample B, it is essential to investigate the carrier concentrations and R_{rad} amid a wider IAC grading range for optimum configuration. Thus, the end Al composition of the IAC grading is varied from 0.61 to 0.75 with the step of 0.02, while keeping the starting Al composition (0.60) and the QB thickness (12 nm) the same. The peak electron and hole concentrations and radiative recombination rates in the middle QW of the active region are shown in Figure 5(a). The effects of the IAC grading (Sample B) are two folds as compared with the fixed-composition QB (Sample A): the QB valence and conduction bands become flatter and steeper, respectively. It is straightforward to understand that the effects are proportional to the IAC grading range since the QB thickness remains the same. In Figure 5(a), $[N_{QW}]$ reduces slowly with the end Al compositions of 0.61–0.71 reflecting the electron containing capability, albeit the reducing rate is small since the large electron mobility can compensate increase of the QB valence band slope. However, the decrease of $[N_{QW}]$ accelerates when the end composition is larger than 0.71, where the QB conduction band becomes too steep for electron transport which equals to greater electron containing capability. For $[P_{QW}]$, it increases quickly in a linear manner as the QB valence band flattens before saturating at higher end compositions above 0.71, showing that the IAC grading can greatly facilitate hole transport and injection.

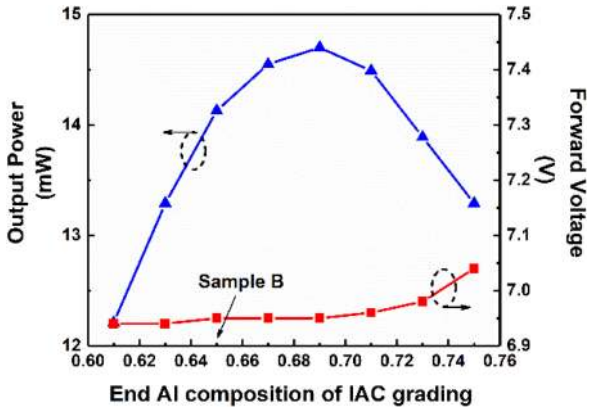

Fig. 6. Output power and forward voltage as a function of the end Al composition of IAC grading.

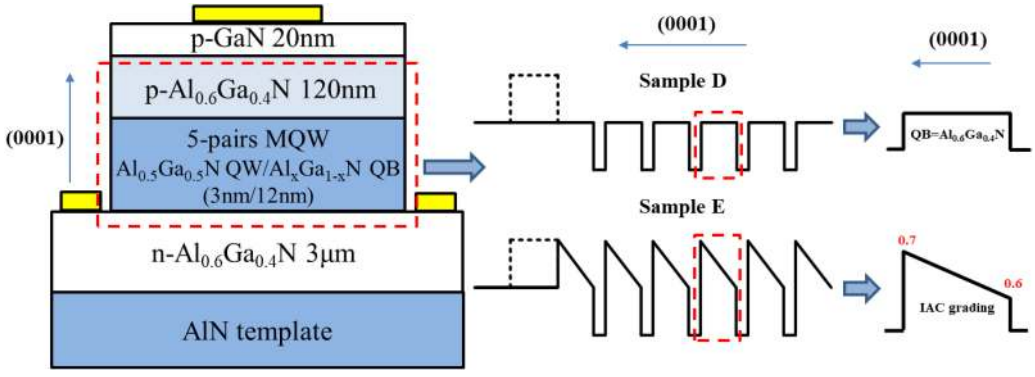

Fig. 7. The cross-sectional schematics and Al composition profiles of EBL-free DUV LEDs emitting at ~270 nm with fixed composition QBs (Sample D) and IAC grading QBs (Sample E). The dashed boxes indicate the assumed position of the EBLs that are not included here.

Figure 5(b) shows the overflown electron concentration [$N_{p-AlGaN}$] in the p-type $Al_{0.6}Ga_{0.4}N$ layer with four end compositions of the IAC grading: 0.60 (i.e., no grading, Sample A), 0.65 (i.e., Sample B), 0.70, and 0.75. [$N_{p-AlGaN}$] reduces significantly by more than one-order-of-magnitude with the increasing end composition from 0.60 to 0.70, indicating greatly-strengthened electron containing capability with steeper QB conduction band due to the IAC grading. Also, it is notable that [$N_{p-AlGaN}$] does not reduce further by too much when increasing the end composition from 0.70 to 0.75 which suggests that the two grading ranges have similar electron containing capability. R_{rad} is shown in Figure 5(a). It first increases and peaks at the end composition of 0.67, coinciding with both high [N_{QW}] and [P_{QW}] before dropping. The forward voltage and output power of the DUV LEDs at 90 mA as a function of the IAC ending composition are shown in Figure 6. With higher end Al composition and thus enhanced electron containing capability, the forward voltage barely increases, which is important and meaningful for the pursuit of high WPE. The change trend of the output power is consistent with that of R_{rad} which peaks at the end composition of 0.69. The slight difference in the end compositions between the peaks of R_{rad} (0.67) of Figure 5(a) and the output power (0.69) of Figure 6 is caused by that R_{rad} is extracted from the middle QW, while the output power integrates the emission from the entire active region of the device.

3. EBL-Free DUV LED

Motivated by the electron containing capability of the QB IAC grading, EBL-free DUV LED structures are designed for further studies as shown in Figure 7. Sample D is modified from Sample A by

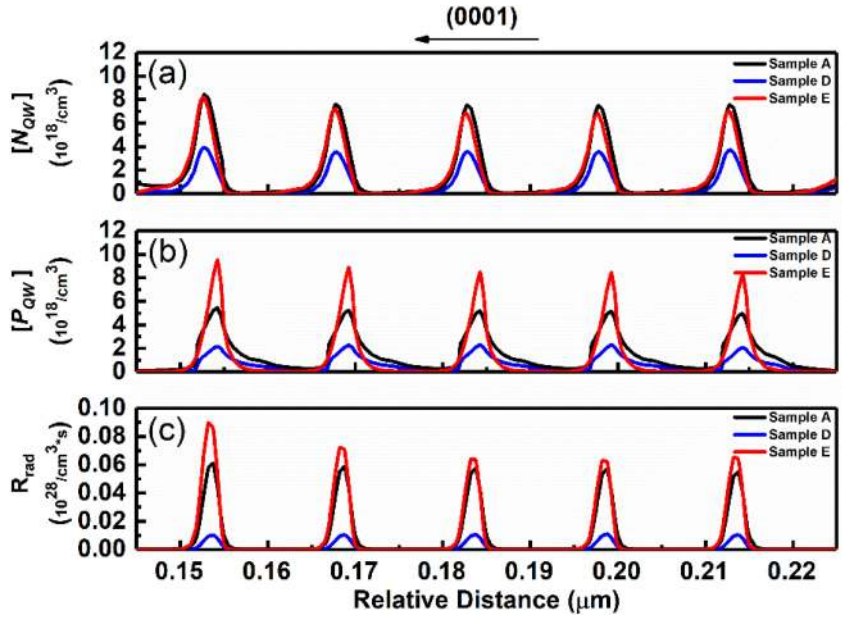

Fig. 8. (a) Electron concentration [N_{QW}], (b) hole concentration [P_{QW}], and (c) radiative recombination rate R_{rad} in the QWs of Samples A, D, and E at 90 mA.

removing the EBL while using a 20-nm thicker p-$Al_{0.6}Ga_{0.4}N$ (120 nm) to compensate the removal of the EBL (20 nm). Sample E has the same structure as Sample D except that IAC grading is applied to QBs with the starting and end compositions of 0.60 and 0.70, respectively.

Figure 8(a) and (b) show the electron concentration [N_{QW}] and the hole concentration [P_{QW}] in the QWs of Samples D and E, with the addition of Sample A as reference. On one hand, [P_{QW}] of Sample E is higher than that of Sample A, thanks to the IAC grading, resembling the situation of Sample B. On the other hand, [N_{QW}] of Sample E is slightly lower than that of Sample A, which is consistent with the observation of Figure 5(a) due to steeper QB valence band. [N_{QW}] and [P_{QW}] of Sample D are significantly lower than those of Sample A, as the removal of the EBL leads to severe electron leakage into the p-type region that not only reduces [N_{QW}] but also compromises hole injection into the QWs. Consequently, Sample D exhibits the lowest radiative recombination rate R_{rad}, as shown in Figure 8(c). Moreover, R_{rad} of Sample E is higher than that of Sample A due to higher [P_{QW}], indicating that the EBL-free DUV LED can have R_{rad} higher than the conventional DUV LED with the fixed-composition AlGaN EBL.

Figure 9(a) provides additional evidence for the excellent electron containing capability of the QB IAC grading. It shows that the overflown electron concentration in the p-$Al_{0.6}Ga_{0.4}N$ layer [$N_{p-AlGaN}$] of Sample E without the EBL is similar to that of Sample A with the EBL in the center of the p-$Al_{0.6}Ga_{0.4}N$ layer, both being close to 1×10^{15} /cm^3. Not surprisingly, Sample D has much larger [$N_{p-AlGaN}$] due to the lack of the EBL versus Sample A. Figure 9(b) further resonates with Figure 8(c). The output power of Sample D without the EBL is very low, because the overflow of electrons into the p-type region is severe, causing poor injection for both electrons and holes. The high electron leakage can be greatly alleviated by adding an EBL such as in Sample A, reaffirming the importance of the EBL in conventional III-nitride DUV LEDs. More importantly, Figure 9(b) indicates that higher (13.5% higher at 90 mA) output power than that of the conventional DUV LED (Sample A) can be achieved by utilizing the electron containing capability of the IAC QB even without the EBL (Sample E). Moreover, the forward voltage of Sample E is slightly lower (1.2% lower at 90 mA) than that of Sample A, while that of Sample D is the lowest due to the EBL removal. With the structures of Samples A and E, one could argue that the results are not unexpected because the last quantum barrier (LQB) reaches Al composition of 0.7 after grading, which is the same Al

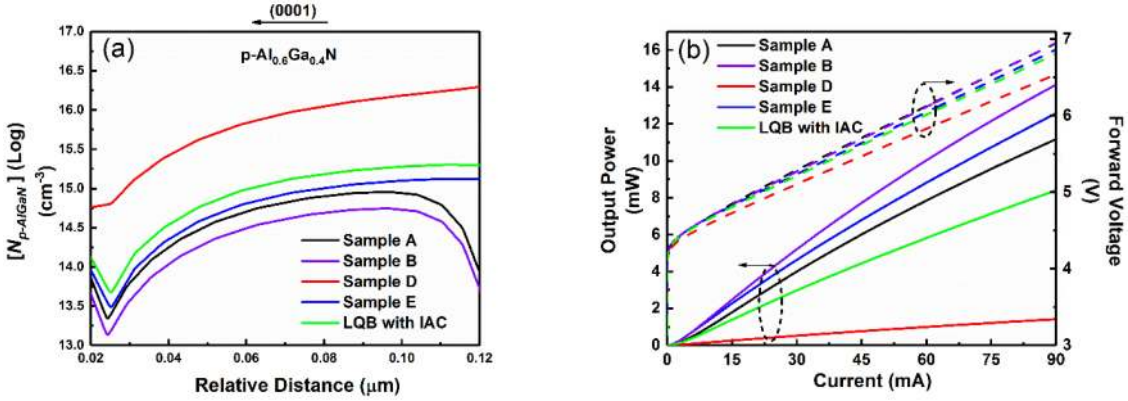

Fig. 9. (a) Electron concentration in the p-$Al_{0.6}Ga_{0.4}N$ layer [$N_{p-AlGaN}$] of Samples D, E and only LQB with IAC structure at 90 mA. (b) Output power and forward voltage as a function of current of Samples, E and only LQB with IAC structure. The forward voltage curve of Sa1mple A (black dash line) overlaps with that of Sample B (violet dash line). Samples A and B are included in (a) and (b) for reference. [$N_{p-AlGaN}$] of Samples A and B are lower in the first 20 nm of the p-$Al_{0.6}Ga_{0.4}N$ layer because of the EBL.

composition as the EBL of Sample A. To confirm, another sample is included based on Sample E except that the IAC grading only applies to LQB (0.6→0.7) and the other four QBs have a flat Al composition of 0.6. As shown in Figure 9(a) and (b), this sample exhibits worse electron containing capability and much lower output power than Samples A and E, thereby suggesting that the EBL design requires the application of the IAC grading to all QBs to realize optimized electron containing and hole injection. Nevertheless, the DUV LED without the p-type EBL is feasible, which could avoid the issues related to the EBL especially p-type doping, hole injection, and epitaxial complexity.

4. Conclusion

To eliminate issues related to the p-type Al-rich EBL including p-doping difficulty, valence band barrier, and epitaxial complexity, we propose the EBL-free AlGaN DUV LED by shifting the paradigm from electron blocking in the p-type region to electron containing in the active region. By employing the linearly-graded-composition AlGaN QB, the carrier concentration in the QWs and overflown electron concentration in the p-type region can be significantly changed due to variation of the slope of the QB conduction and valence bands and thus carrier transport barrier. This can further result in modification of the radiative recombination rate. Specially, when grading the Al composition of the AlGaN QB from low to high along the growth direction, i.e., the *c*-axis, the active region exhibits the remarkable electron containing capability that reduces the electron overflow. In addition, the hole injection and thus hole concentration increases in the QW due to flattering of the QB valence band and thus lower hole transport barrier, that can enhance the radiative recombination rate. For two DUV LEDs emitting at 270 nm, the EBL-free one with the graded $Al_xGa_{1-x}N$ ($x = 0.60 \rightarrow 0.70$) QBs exhibits similar degree of electron overflow ($\sim 1 \times 10^{15}$ /cm^3) and higher hole concentration in the QWs simultaneously, leading to 13.5% higher output power as compared with the other conventional one with the p-type EBL. As the proposed paradigm is straightforward and effective, this work can inspire the DUV LED and laser community to incorporate the electron containing capability in the device design to replace or complement the p-type EBL. Besides, the proposed paradigm can be applied to III-nitride light emitters of other spectral ranges.

Although this is a theoretical work focusing on the paradigm of the electron containing capability and the validity of the proposed EBL-free DUV LED concept, we expect that the experimental implementation would be relatively straightforward. This is because the grading rate of the 10% compositional change in a 12 nm AlGaN layer (Sample E) can be realized by mainstream epitaxial technologies such as metal organic chemical vapor deposition (MOCVD) and molecular beam

epitaxy (MBE) as shown by various reports [48]–[52]. Since the compositional change is relatively small and no intentional doping is needed amid the QB growth, for instance, the grading can be achieved by varying Al/III molar ratio in a MOCVD process. This study shows that the DUV LED without the EBL can achieve slightly better output power (i.e., WPE) performance, as opposed to the conventional DUV LED. However, in practice ones can optionally combine both the QB IAC grading and the EBL to obtain even less electron spill-over [Figure 9(a)] and higher output power [Figure 9(b)] as shown by Sample B. It should be noted that the inclusion of the EBL will inevitably increase the forward voltage as exhibited by Sample B in Figure 9(b) as well as epitaxial and doping difficulty, especially when the goal is to make shorter-wavelength DUV LED. Therefore, ones can make the proper choice and compromise amid the device design processes.

References

[1] M. Shatalov *et al.*, "AlGaN deep-ultraviolet light-emitting diodes with external quantum efficiency above 10%," *Appl. Phys. Exp.*, vol. 5, no. 8, 2012, Art. no. 082101.

[2] T. Takano, T. Mino, J. Sakai, N. Noguchi, K. Tsubaki, and H. Hirayama, "Deep-ultraviolet light-emitting diodes with external quantum efficiency higher than 20% at 275 nm achieved by improving light-extraction efficiency," *Appl. Phys. Exp.*, vol. 10, no. 3, 2017, Art. no. 031002.

[3] S. M. Sze, *Physics of Semiconductor Devices*, 2nd ed. Hoboken, NJ, USA: Wiley, 1981.

[4] S. Shervin *et al.*, "Flexible deep-ultraviolet light-emitting diodes for significant improvement of quantum efficiencies by external bending," *J. Phys. D, Appl. Phys.*, vol. 51, no. 10, 2018, Art. no. 105105.

[5] M. H. Kim *et al.*, "Origin of efficiency droop in GaN-based light-emitting diodes," *Appl. Phys. Lett.*, vol. 91, 2007, Art. no. 183507.

[6] Y.-K. Kuo, J.-Y. Chang, and M.-C. Tsai, "Enhancement in hole-injection efficiency of blue InGaN light-emitting diodes from reduced polarization by some specific designs for the electron blocking layer," *Opt. Lett.*, vol. 35, pp. 3285–3287, 2010.

[7] H. Hirayama, Y. Tsukada, T. Maeda, and N. Kamata, "Marked enhancement in the efficiency of deep-ultraviolet AlGaN light-emitting diodes by using a multiquantum-barrier electron blocking layer," *Appl. Phys. Exp.*, vol. 3, no. 3, 2010, Art. no. 031002.

[8] H. Sun *et al.*, "Band alignment of $B_{0.14}Al_{0.86}N/Al_{0.7}Ga_{0.3}N$ heterojunction," *Appl. Phys. Lett.*, vol. 111, 2017, Art. no. 122106.

[9] L. Li, Y. Zhang, S. Xu, W. Bi, Z. H. Zhang, and H. C. Kuo, "On the hole injection for III-nitride based deep ultraviolet light-emitting diodes," *Materials*, vol. 10, 2017, Art. no. 1221.

[10] Z.-H. Zhang *et al.*, "Nearly efficiency-droop-free AlGaN-based ultraviolet light-emitting diodes with a specifically designed superlattice p-type electron blocking layer for high Mg doping efficiency," *Nanoscale Res. Lett.*, vol. 13, 2018, Art. no. 122.

[11] M. L. Nakarmi, N. Nepal, J. Y. Lin, and H. X. Jiang, "Photoluminescence studies of impurity transitions in Mg-doped AlGaN alloys," *Appl. Phys. Lett.*, vol. 94, 2009, Art. no. 091903.

[12] H. Hirayama, N. Noguchi, T. Yatabe, and N. Kamata, "227 nm AlGaN light-emitting diode with 0.15 mW output power realized using a thin quantum well and AlN buffer with reduced threading dislocation density," *Appl. Phys. Exp.*, vol. 1, no. 5, 2008, Art. no. 051101.

[13] S. I. Inoue, N. Tamari, and M. Taniguchi, "150 mW deep-ultraviolet light-emitting diodes with large-area AlN nanophotonic light-extraction structure emitting at 265 nm," *Appl. Phys. Lett.*, vol. 110, 2017, Art. no. 141106.

[14] Y. A. Yin, N. Wang, S. Li, Y. Zhang, and G. Fan, "Advantages of deep-UV AlGaN light-emitting diodes with an AlGaN/AlGaN superlattices electron blocking layer," *Appl. Phys. A*, vol. 119, pp. 41–44, 2015.

[15] Y. Zhang *et al.*, "The improvement of deep-ultraviolet light-emitting diodes with gradually decreasing Al content in AlGaN electron blocking layers," *Superlattices Microstruct.*, vol. 82, pp. 151–157, 2015.

[16] X. Fan *et al.*, "Efficiency improvements in AlGaN-based deep ultraviolet light-emitting diodes using inverted-V-shaped graded Al composition electron blocking layer," *Superlattices Microstruct.*, vol. 88, pp. 467–473, 2015.

[17] Z.-H. Zhang *et al.*, "Hole transport manipulation to improve the hole injection for deep ultraviolet light-emitting diodes," *ACS Photon.*, vol. 4, pp. 1846–1850, 2017.

[18] J. Simon, V. Protasenko, C. X. Lian, H. L. Xing, and D. Jena, "Polarization-induced hole doping in wide-bandgap uniaxial semiconductor heterostructures," *Science*, vol. 327, pp. 60–64, 2010.

[19] L. Zhang *et al.*, "Three-dimensional hole gas induced by polarization in (0001)-oriented metal-face III-nitride structure," *Appl. Phys. Lett.*, vol. 97, 2010, Art. no. 062103.

[20] B. Cheng *et al.*, "Enhanced vertical and lateral hole transport in high aluminum-containing AlGaN for deep ultraviolet light emitters," *Appl. Phys. Lett.*, vol. 102, 2013, Art. no. 231106.

[21] Y. Chen *et al.*, "High hole concentration in p-type AlGaN by indium-surfactant-assisted Mg-delta doping," *Appl. Phys. Lett.*, vol. 106, 2015, Art. no. 162102.

[22] J. Li, W. Yang, S. Li, H. Chen, D. Liu, and J. Kang, "Enhancement of p-type conductivity by modifying the internal electric field in Mg-and Si-δ-codoped $Al_xGa_{1-x}N/Al_yGa_{1-y}N$ superlattices," *Appl. Phys. Lett.*, vol. 95, 2009, Art. no. 151113.

[23] Y. Aoyagi, M. Takeuchi, S. Iwai, and H. Hirayama, "High hole carrier concentration realized by alternative co-doping technique in metal organic chemical vapor deposition," *Appl. Phys. Lett.*, vol. 99, 2010, Art. no. 112110.

[24] L. Lu *et al.*, "Performance improvement of AlGaN-based deep-ultraviolet light-emitting diodes via asymmetric step-like AlGaN quantum wells," *Superlattices Microstruct.*, vol. 104, pp. 240–246, 2017.

[25] F. Wu *et al.*, "Significant internal quantum efficiency enhancement of GaN/AlGaN multiple quantum wells emitting at ~350 nm via step quantum well structure design," *J. Phys. D, Appl. Phys.*, vol. 50, no. 24, 2017, Art. no. 245101.
[26] L. Lu, Y. Zhang, F. Xu, G. Ding, and Y. Liu, "Performance improvement of AlGaN-based deep-ultraviolet light-emitting diodes via Al-composition graded quantum wells," *Superlattices Microstruct.*, vol. 118, pp. 55–60, 2018.
[27] X. Bao, P. Sun, S. Liu, C. Ye, S. Li, and J. Kang, "Performance improvements for AlGaN-based deep ultraviolet light-emitting diodes with the p-type and thickened last quantum barrier," *IEEE Photon. J.*, vol. 7, no. 1, Feb. 2015, Art. no. 1400110.
[28] S. Chen *et al.*, "Numerical analysis on the effects of multi-quantum last barriers in AlGaN-based ultraviolet light-emitting diodes," *Appl. Phys. A*, vol. 118, pp. 1357–1363, 2015.
[29] J.-Y. Chang, H.-T. Chang, Y.-H. Shih, F.-M. Chen, M.-F. Huang, and Y.-K. Kuo, "Efficient carrier confinement in deep-ultraviolet light-emitting diodes with composition-graded configuration," *IEEE Trans. Electron Devices*, vol. 64, no. 12, pp. 4980–4984, Dec. 2017.
[30] L. He *et al.*, "Performance enhancement of AlGaN-based 365 nm ultraviolet light-emitting diodes with a band-engineering last quantum barrier," *Opt. Lett.*, vol. 14, no. 26, pp. 17977–17987, 2018.
[31] J.-Y. Chang and Y.-K. Kuo, "Advantages of blue InGaN light-emitting diodes with composition-graded barriers and electron-blocking layer," *Phys. Status Solidi A*, vol. 110, pp. 1103–1106, 2013.
[32] Y.-A. Chang, J.-Y. Chang, Y.-T. Kuo, and Y.-K. Kuo,"Investigation of green InGaN light-emitting diodes with asymmetric AlGaN composition-graded barriers and without an electron blocking layer," *Appl. Phys. Lett.*, vol. 100, 2012, Art. no. 251102.
[33] C. H. Wang *et al.*, "Hole transport improvement in InGaN/GaN light-emitting diodes by graded-composition multiple quantum barriers," *Appl. Phys. Lett.*, vol. 99, 2011, Art. no. 171106.
[34] T. Kinoshita, T. Obata, H. Yanagi, and S.-I. Inoue, "High p-type conduction in high-Al content Mg-doped AlGaN," *Appl. Phys. Lett.*, vol. 102, 2013, Art. no. 012105.
[35] M. L. Nakarmi, K. H. Kim, M. Khizar, Z. Y. Fan, J. Y. Lin, and H. X. Jiang, "Electrical and optical properties of Mg-doped $Al_{0.7}Ga_{0.3}N$ alloys," *Appl. Phys. Lett.*, vol. 86, 2005, Art. no. 092108.
[36] S. Nikzad *et al.*, "Single photon counting UV solar-blind detectors using silicon and III-nitride materials," *Sensors*, vol. 16, 2016, Art. no. 927.
[37] R. Collazo *et al.*, "Progress on n-type doping of AlGaN alloys on AlN single crystal substrates for UV optoelectronic applications," *Phys. Status Solidi C*, vol. 8, no. 7/8, pp. 2031–2033, 2011.
[38] APSYS, Crosslight Software Inc., Burnaby, BC, Canada. [Online]. Available: http://www.crosslight.com
[39] S. L. Chuang and C. S. Chang, "K· p method for strained wurtzite semiconductors," *Phys. Rev. B*, vol. 54, pp. 2491–2504, 1996.
[40] S. L. Chuang and C. S. Chang, "A band-structure model of strained quantum-well wurtzite semiconductors," *Semicond. Sci. Technol.*, vol. 12, pp. 252–263, 1997.
[41] G.-D. Hao, M. Taniguchi, N. Tamari, and S.-I. Inoue, "Current crowding and self-heating effects in AlGaN-based flip-chip deep-ultraviolet light-emitting diodes," *J. Phys. D, Appl. Phys.*, vol. 51, no. 3, 2018, Art. no. 035103.
[42] R. Collazo *et al.*, "Progress on n-type doping of AlGaN alloys on AlN single crystal substrates for UV optoelectronic applications," *Phys. Status Solidi C*, vol. 8, pp. 2031–2033, 2011.
[43] E.A. Shevchenkoa *et al.*, "AlGaN quantum well heterostructures for mid-ultraviolet emitters with improved room temperature quantum efficiency," *Acta Physica Polonica A*, vol. 126, pp. 1140–1142, 2014.
[44] P. Kozodoy, H. Xing, S. P. DenBaars, and U. K. Mishra, "Heavy doping effects in Mg-doped GaN," *J. Appl. Phys.*, vol. 87, pp. 1832–1835, 2000.
[45] J. Yun, J.-I. Shim, and H. Hirayama, "Analysis of efficiency droop in 280 nm AlGaN multiple-quantum-well light-emitting diodes based on carrier rate equation," *Appl. Phys. Exp.*, vol. 8, 2015, Art. no. 022104.
[46] C. Coughlan, S. Schulz, M. A. Caro, and E. P. O'Reilly, "Band gap bowing and optical polarization switching in $Al_{1-x}GaxN$ alloys," *Phys. Status Solidi B*, vol. 252, pp. 879–884, 2015.
[47] A. Punya and W. R. L. Lambrecht, "Valence band effective-mass Hamiltonians for the group-III nitrides from quasiparticle self-consistent GW band structures," *Phys. Rev. B*, vol. 85, 2012, Art. no. 195147.
[48] P. S. Park, D. N. Nath, S. Krishnamoorthy, and S. Rajan, "Electron gas dimensionality engineering in AlGaN/GaN high electron mobility transistors using polarization," *Appl. Phys. Lett.*, vol. 100, 2012, Art. no. 063507.
[49] L. Ardaravičius, O. Kiprijanovič, and J. Liberis, "Electron velocity enhancement in polarization-doped AlGaN," *Mater. Sci.*, vol. 19, pp. 129–133, 2013.
[50] Z. H. Wu, F. A. Ponce, J. Hertkorn, and F. Scholz, "Determination of the electronic band structure for a graded modulation-doped Al GaN/AlN/GaN superlattice," *Appl. Phys. Lett.*, vol. 91, 2007, Art. no. 142121.
[51] S. Bajaj, F. Akyol, S. Krishnamoorthy, Y. Zhang, and S. Rajan, "AlGaN channel field effect transistors with graded heterostructure ohmic contacts," *Appl. Phys. Lett.*, vol. 109, 2016, Art. no. 133508.
[52] Y. L. Fang *et al.*, "High linearity step-graded AlGaN/GaN heterojunction field effect transistor," in *Proc. 13th China Int. Forum Solid State Lighting, Int. Forum Wide Bandgap Semicond. China*, 2016, pp. 104–106.